7

Fictive temperature measurements in silica-based optical fibers and its application to Rayleigh loss reduction

Matthieu Lancry[1], Elise Régnier[2] and Bertrand Poumellec[1]
(1) Institut de Chimie Moléculaire et des Matériaux d'Orsay, Laboratoire de Physico-chimie de l'Etat Solide, UMR CNRS-UPS 8182, Université Paris Sud 11, Bâtiment 410, 91405 Orsay, France
(2) Draka Communications, Centre Data 4, Route de Nozay, 91460 Marcoussis, France

1. Introduction

For many applications, silica is the preferred material, providing excellent physical and chemical properties such as optical transparency from IR to UV range, a low thermal expansion coefficient, and a high resistance to laser induced damage. Silica-based glasses thus provide the backbone for many of today's rapidly expanding photonics applications across fields such as optical telecommunications, electronics, sensor technologies, medical applications, and materials processing.
Thus, numerous elaboration methods are used to produce v-silica-based devices. For example, the technique of vapor phase deposition i.e. Axial Deposition (VAD), Outside Vapor Deposition (OVD), Modified Chemical Vapor Deposition (MCVD), Plasma Enhanced Chemical Vapor Deposition (PECVD) is common in the fabrication of most standard telecommunication silica-based fibers or planar waveguides (Miller and Chynoweth 1979). Furthermore, other processes including sol-gel synthesis (Simmons-Potter, Potter Jr et al. 1996) or conventional melting of raw materials are routinely used to manufacture optical fibers. As a result of this large variety of elaboration processes, all the SiO_2-based glasses are different in terms of chemical composition and structural disorder (Hosono, Ikuta et al. 2001). One way to characterize the glass structural disorder is to determine the fictive temperature T_f.
As described in section 2, it is well known that the fictive temperature is linked to various glass properties such as density (Bruckner 1970; Agarwal and Tomozawa 1997), mechanical fatigue resistance (Bruckner 1970; Agarwal and Tomozawa 1997) or Rayleigh scattering loss (Saito, Kakiuchida et al. 1998). From optical fiber manufacturing point of view, monitoring the fictive temperature is thus a quick and reliable way to optimize the manufacturing process in order to reduce the Rayleigh scattering loss which is the major source of loss in telecommunication optical fibers. For a single mode telecommunication fiber, this corresponds to 90% loss at 1310nm and 80% at 1550nm (e.g. 0.16dB/km for a total of 0.19dB/km).

As recently reported in several papers (Agarwal, Davis et al. 1995; Champagnon, Chemarin et al. 1998; Le Parc 2002; Helander 2004; Koike, Ryu et al. 2005), the fictive temperature T_f of silica based glasses can be determined easily and in a reliable manner by Fourier Transform Infra-Red spectroscopy (FTIR) or Raman scattering spectroscopy. In these methods, scientists use an empirical relation that exists between the wavenumber, width or intensity of silica structural bands and the fictive temperature. Section 3 provides an overview of these methods.
However, one problem is that the features of the silica bands (position, intensity and width) vary not only with T_f but also with the elaboration process and the material composition (Agarwal and Tomozawa 1995; Kim, Tomozawa et al. 2001; Lancry, Flammer et al. 2007; Lancry, Flammer et al. 2007). This is an issue as the chemical composition of a fiber is not constant throughout its cross section but varies for designing the desired refractive index profile for a targeted application e.g. Single Mode Fiber (SMF), Multi-Mode Fiber (MMF), Pure Silica Core Fiber (PSCF), Dispersion Compensating Fiber (DCF), Dispersion Shifted Fiber (DSF). Thus, calibration curves between T_f and the IR band peak characteristics (position, intensity, width) are needed for each material composition (F, P, Ge…). In section 4, we will present an overview of all calibration curves found in the literature together with the method to realize such calibration curves.
An other important parameter that has to be taken into account is that, in general, a glass sample can exhibit different fictive temperatures at its surface and in bulk. This situation can occur, for example, when a glass is rapidly cooled from the liquid state, as it is done in fiber production. In this case, a higher T_f is expected at the fiber surface than in the bulk due to a faster cooling rate at the surface (Peng, Agarwal et al. 1997; Lancry, Flammer et al. 2007). One objective of section 5 is to examine this phenomenon in conventional optical fibers.

Minimizing the optical losses in fibers is a recurrent target for fiber manufacturers. In literature, two approaches have been proposed to reduce Rayleigh scattering loss in silica-based fibers via a reduction of T_f. Indeed, we can optimize the core and/or cladding chemical compositions (Kakiuchida, Sekiya et al. ; Tajima, Ohashi et al. 1992; Lines 1994; Saito and Ikushima 1998; Saito, Kakiuchida et al. 1998; Tsujikawa, Tajima et al. 2000; Kakiuchida, Saito et al. 2002; Saito and Ikushima 2002; Kakiuchida, Saito et al. 2003; Saito, Yamaguchi et al. 2004), or optimize the thermal conditions of the fiber drawing (Todoroki and Sakaguchi 1997; Sakaguchi and Todoroki 1998; Sakaguchi 2000; Tsujikawa, Tajima et al. 2000; Tsujikawa, Tajima et al. 2005). These two approaches are discussed in section 6.

This paper will thus give an overview of methods to measure the fictive temperature in silica-based optical fibers. We will first recall what is T_f in section 2. We will see that both Raman and IR spectroscopies can be used (Section 3). We will also show in section 4 that measuring T_f f in optical fibers requires taking many corrections into account. Section 5 will thus give some examples of T_f profiles measured in optical fibers manufactured in different conditions. Finally, section 6 will present two approaches to reduce Rayleigh scattering loss in silica-based fibers via a reduction of T_f.

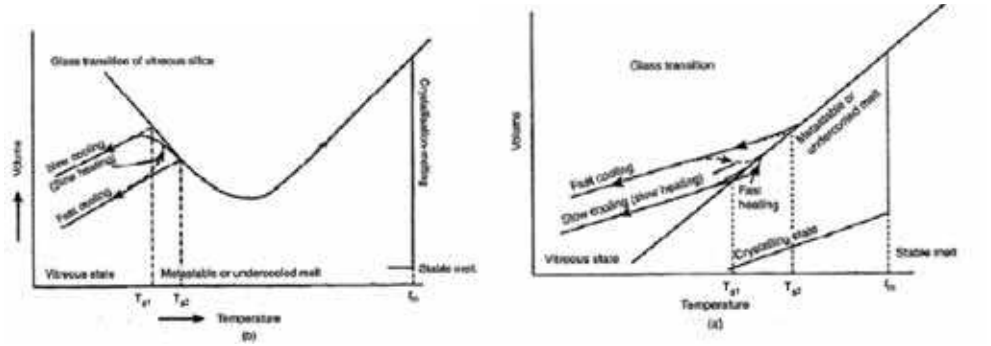

Fig. 1. Schematic diagram of specific volume-temperature relations for a) a normal glass and b) silica glass in the anomalous region (Bruckner 1970).

2. What is the fictive temperature T_f?

2.1 Definition

Glass is not merely a super-cooled liquid. The volume-temperature diagram shown in Fig. 1a illustrates this distinction. When a liquid is cooled, it crystallizes at or slightly below the melting point. If there are not enough crystal nuclei or if the viscosity is too high to allow sufficient crystallization rates, under-cooling of the liquid can occur. However, in the case of a glass, the viscosity of the liquid rapidly increases with decreasing temperature, and atomic rearrangement slows down more than would be typical for the super-cooled liquid. These observations result in the deviation from the metastable equilibrium curve as it can be seen in Fig. 1a. This change in slope is characteristic of a glass. The cooling rate determines the knee position when the deviation (from the extrapolated liquid curve) begins to occur. Slower cooling, for instance, results in a smaller deviation from the extrapolated liquid curve. Figure 1 shows that the point of intersection of the two slopes defines a transformation point i.e. glass-transition temperature (T_g), which depends on the cooling rate. Practical limitation on cooling rate defines the transformation range [T_{g1}-T_{g2}] in which the cooling rate can affect the structure-sensitive properties such as density or refractive index. The structure, which is frozen-in during the glass transformation, persists at all lower temperatures. Thus, a glass has a configurational temperature or fictive temperature that may differ from its T_g. **The fictive temperature is the temperature at which the glass structure is frozen. It describes thus the structure of a glass and is related to the cooling rate. A fast-quenched glass will have a higher fictive temperature than a slowly cooled glass.**

	Increase in fictive temperature
Density	↑ (T< 1773 K);↓ (T>1773K) [Bruckner 1970; Fraser 1968; Shackelford, Masaryl et al. 1970; Zarzycki 1982; Hong 2003]
Refractive index	↑ [Bruckner 1970]
Viscosity	↓ [Hetherington 1964; Hong 2003]
Thermal expansion α	↑ [Bruckner 1970]
Etch rate	↑ [Agarwal 1997]
Water diffusion	↓ [Roberts 1966]
Compressibility	↓ [Fraser 1968]
Shear modulus	↓ [Fraser 1968]
Young's modulus	↑ [Fraser 1968]
Rayleigh scattering	↑ [Pinnow, Candau et al. 1968; Pinnow, Candau et al. 1968; Lines 1984; Sakaguchi and Todoroki 1998; Kakiuchida, Saito et al. 2003; Tsujikawa, Tajima et al. 2005; Le Parc 2002, Champagnon 2000]

Table 1. Qualitative behavior of the effect of fictive temperature increase on silica glass structure and properties (1273K < T < 1873K). Adapted from Ref. (Agarwal and Tomozawa 1997).

2.2 Qualitative link between fictive temperature and properties of silica glass

Given a well defined chemical composition, silica glass can have different structures and properties depending upon its thermal history (Bruckner 1970; Agarwal, Davis et al. 1995). This is attributed to different fictive temperatures. Thus, the fictive temperature allows learning about glass properties such as density, refractive index, hardness, mechanical strength and chemical durability. In this section, the changes in various properties of silica glasses induced by thermal or mechanical processes reported in the literature are compared. These observations are summarized in Table 1 (adapted from (Agarwal and Tomozawa 1997)). The structural changes induced by modification of fictive temperature are considered in the anomalous region. This anomalous region is the range of fictive temperatures from 1273K to 1773K, where the density of silica glass increases with increasing fictive temperature (Fraser 1968; Bruckner 1970; Shackelford, MASARYK et al. 1970; Zarzycki 1982). This is the opposite to what happens in the other glasses. This is illustrated in Fig. 1b. In addition, Fig. 2 shows the density according to T_f for such silica glasses.

As it can be seen in Table 1, a glass with a higher fictive temperature has larger light scattering loss, larger mechanical fatigue resistance, lower viscosity and larger HF etching rate. Concerning the fiber drawing parameters, fictive temperature of fiber core and inner cladding is higher for fibers processed with a faster cooling rate, which generally corresponds to higher drawing speed or lower tension force.

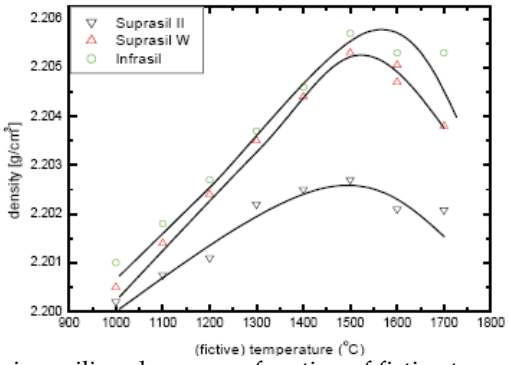

Fig. 2. Densities of various silica glasses as a function of fictive temperature (Bruckner 1971) in the anomalous region.

As this paper is dedicated to fictive temperature in optical fibers, in the following we briefly discuss the **relationship that is well known between Rayleigh scattering and fictive temperature** to estimate the intrinsic loss of silica-based fibers (Saito, Kakiuchida et al. 1998). The Rayleigh scattering coefficient R (dB/km/μm⁴) is expressed as the sum of two contributions R_ρ and R_c which are the Rayleigh scattering coefficients resulting from density fluctuations and concentration fluctuations, respectively. R_c is assumed to be independent on T_f (Martinez and Angell 2002) as it is mainly governed by dopant concentration fluctuations (e.g. polarizability differences between dopants and host material) arising from the elaboration process (e.g. higher concentration fluctuations in VAD process when compared to MCVD process (Dalle)) and the thermodynamics.

$$R_\rho = \frac{8}{3}\pi^3 n^8 p^2 k_B \beta_T T_f \tag{1}$$

R_ρ is expressed as Eq. (1), where n is the refractive index, p the average photo-elastic coefficient, T_f the fictive temperature, and β_T the isothermal compressibility for a given fictive temperature. This equation highlights the strong impact of n and T_f on the Rayleigh scattering. Equation (1) indicates that R_ρ is proportional to T_f (Pinnow, Candau et al. 1968; Pinnow, Candau et al. 1968; Lines 1984). This is indeed confirmed by experimental results that show that the Rayleigh scattering coefficient has a linear relationship with T_f in pure silica glasses and in fibers which have only density fluctuations (only R_ρ) (Sakaguchi and Todoroki 1998; Kakiuchida, Saito et al. 2003). Usually, for low dopant concentrations (case of most SMFs used in telecommunications), Rayleigh scattering is mainly caused by frozen-in density fluctuations. Figure 3 shows the relationship between the R (sum of R_ρ + R_c) value and T_f. The solid and dotted lines express the dependency in the cases of pure silica and slightly GeO_2-doped (typ. 5w %) silica glasses, respectively. In addition, the Rayleigh losses depend strongly on the wavelength (λ^{-4} dependence), that's why telecommunication transmission windows are in the NIR (Near-Infra-Red) range around the minimum attenuation window.

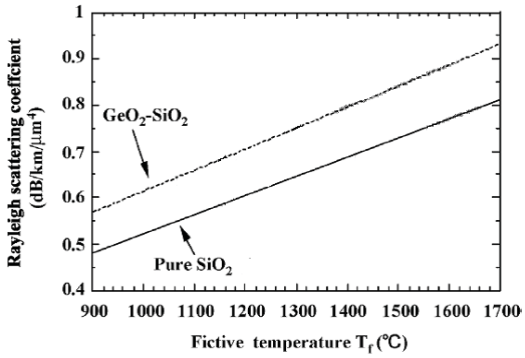

Fig. 3. Relationship between the Rayleigh scattering coefficient and T_f. Extracted from Ref. (Tsujikawa, Tajima et al. 2005).

3. Methods to determine the fictive temperature of silica glasses

3.1 Overview of methods to measure T_f

In principle, fictive temperature of a glass can be determined by measuring any glass properties. In practice, Differential Scanning Calorimetric analysis is a popular method to measure fictive temperature of vitreous materials. However this method cannot be used for silica glasses (and thus optical fibers) since they show a negligible change in specific heat around the glass transition region.

Recently, several authors have reported two methods based on IR absorption (or reflection) and Raman scattering to determine the fictive temperature of silica glass. In these methods, one uses an empirical relation between T_f and the intensity I, wavenumber σ or bandwidth Δσ of silica vibrational structural bands. These correlations are summarized in Table 2 together with the interpretation and the corresponding references. Using these correlations, it is possible to determine the fictive temperature of different types of silica glasses providing that a calibration was previously established.

Method	Observations	References
Raman 440cm^{-1} band	$T_f \uparrow \Rightarrow \sigma\uparrow$ $\Delta\sigma\downarrow$	Le Parc 2002; Galeener 83
Raman D_1 (485 cm^{-1}) band D_2 (600 cm^{-1}) band	$T_f \uparrow \Rightarrow I\uparrow$	Le Parc 2002; Bates 1974; Stolen 1976; Mikkelsen 1980
Raman 800cm^{-1} band	$T_f \uparrow \Rightarrow \sigma\uparrow$	Le Parc 2002; Galeener 1983
Raman 1060/1200cm^{-1} band	$T_f \uparrow \Rightarrow \sigma\downarrow$	Le Parc 2002; Galeener 1983
FTIR, Reflectance 1120cm^{-1}	$T_f \uparrow \Rightarrow \sigma\downarrow$ $\Delta\sigma\uparrow$	Le Parc 2002; Kim 2001; Agarwal 1995; Kim 2001; Peng 1997; Hong 2003; Helander 2004
FTIR, Transmission 2260cm^{-1}	$T_f \uparrow \Rightarrow \sigma\downarrow$	Le Parc 2002; Kim 2001; Hong 2003

Table 2. Relations between fictive temperature and IR absorption and Raman scattering bands' characteristics in pure silica.

On the one hand, Raman scattering method is well adapted to realize T_f cross-section profile in optical fibers and especially in SMF as it provides a good spatial resolution (~ 1μm) (Martinet, Martinez et al. 2008). On the other hand, it has been shown that the IR absorption band located near 1120 cm^{-1}, and which corresponds to the fundamental asymmetric stretching vibration of the Si—O—Si structure, is the most sensitive to structural changes and thus to the T_f changes. This IR vibrational structural band is therefore related to the Si-O-Si bond angle (Bell, Bird et al. 1968; Galeener 1979). In addition, the determination of the peak position is much reliable using FTIR technique. Thus, in the following, the asymmetric bond-stretching vibration observed near 1120 cm^{-1} in the IR reflection spectra is monitored to determine the fictive temperature for several types of silica glasses or optical fibers. As reported in the literature, this method remains well adapted to realize T_f cross-section profiles in optical fibers (Peng, Agarwal et al. 1997; Kim and Tomozawa 2001; Kim, Tomozawa et al. 2001; Hong 2003) as the spatial resolution can be as small as 10 microns. At the opposite, IR transmission measurements are less precise (lower slope of the calibration curve between the peak position and the fictive tempertaure) and require to prepare very thin samples (thinner than 50 μm).

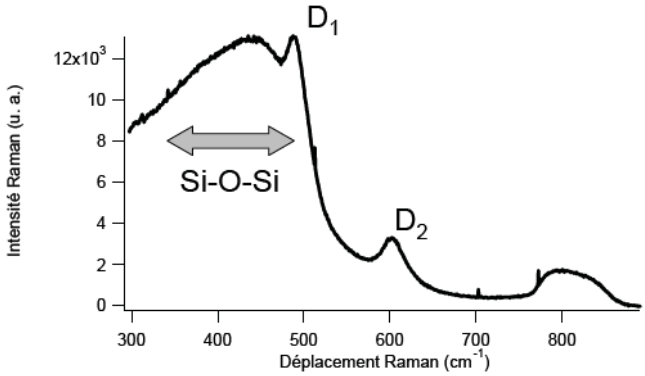

Fig. 4. Typical Raman scattering spectrum of a pure silica glass. Le parc, R. (2002)

An example of the resulting reflectance spectrum is shown in Fig. 5. This spectrum was recorded in a pure silica glass. Typically, there is a predominant IR band at 1120 cm^{-1} accompanied by a shoulder at 1200 cm^{-1}. This shoulder is due to the component which is parallel to the direction of the light propagation (the longitudinal optical, LO mode) while the main band at 1122 cm^{-1} is caused by the transversal optical (TO) mode (Bell, Bird et al. 1968; Galeener 1979).

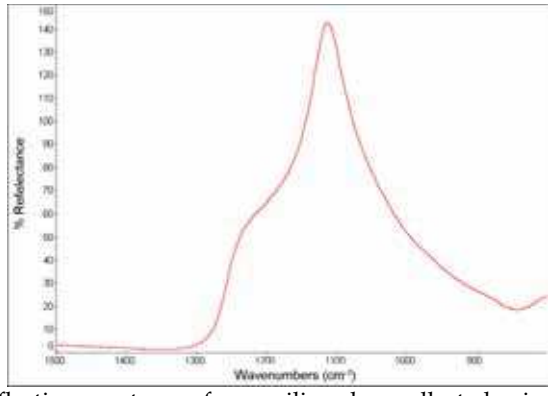

Fig. 5. Typical IR reflection spectrum of pure silica glass collected using Nexus FTIR micro-spectrometer with a maximum reflection angle of 37°.

3.2 Sample preparation, the three investigated methods

Three different methods can be used to determine the fictive temperature of SMF's (Single Mode Fiber) or MMF (Multi-Mode Fiber) cores.

3.2.1 Cleaved fiber and standard FTIR reflection measurements

The fiber was simply cleaved and then mounted vertically in epoxy resin at 90 ± 1 degrees off the horizontal direction using a V-groove metal support. Then, the mounted fiber was etched for 30s in 10% HF-10% H_2SO_4 solution to remove surface water and to reveal boundaries of the core, inner cladding and outer cladding. Figure 6 displays an optical microscope photograph of a SMF made by MCVD process. Thanks to etching we can clearly see the different parts of the fiber such as core, inner-cladding and outer-cladding. Another possibility to reveal core-cladding area will be to observe the samples between cross-polarized. Indeed, due to the chemical composition profile, relative changes in thermal expansion coefficient result in a stress and thus birefringence is radially symmetric (Bachmann, Hermann et al. 1987).

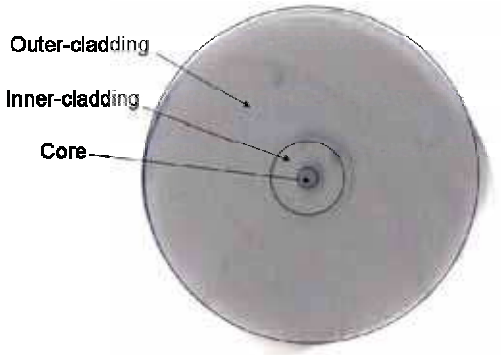

Fig. 6. Optical microscope photograph of SMF after 30 s etching in 10% HF-10% H_2SO_4 solution.

Standard FTIR: Finally, IR reflection spectra were recorded by means of FTIR spectrometer. The spatial resolution can be reduced down to 20 μm x 20 μm. Therefore this technique in well adapted to MMF measurements where the average core diameter is at least 50 microns wide. However in SMF, this results in an average value of T_f including both core and cladding. Since the beam probe size is much larger than the SMF core, it is thus necessary to perform "strong" correction, due to the cladding's impact. This degrades strongly the reproducibility of our measurements.
FTIR with FPA type detector: On the other hand, the FTIR reflection spectra can be recorded by means of a FTIR Spotlight 300 Perkin Elmer equipped with the new technology of FPA (Focal Plane Array) detector. The instrument provides 6:1 imaging on a MCT (Mercury Cadmium Telluride) detector, resulting in a nominal resolution of 8 μm x 8 μm. Using this technique, we are thus able to measure SMF's core only. However, the alignment of the probe beam on the fiber core is quite difficult since the core and pixel size are roughly similar. This can result in less reliable measurements.

Treatment	Time	Diluents
Mounting in epoxy resin	3h	
Polishing with SiC 600	few min	Water
Polishing with SiC 1200	10 min	Water
Polishing with 6 μm diamond slurry	10 min	Oil
Polishing with 1 μm diamond slurry	10 min	Oil
Polishing with 0.25 μm diamond slurry	15 min	Oil
10%HF-10%H_2SO_4 etching	30s	Water

Table 3. Samples treatments before FTIR reflection experiments: mounting, polishing and etching.

3.2.2 Blaze polished fiber and FTIR

Instead of trying to reduce the beam probe size, as shown in the previous section, in the following, the fiber is cleaved and then polished at very small angle (typ. a few degrees), in order to increase the fiber core surface area. In this view, the fibers are mounted in epoxy resin a few degrees off the horizontal direction using a thin taper plastic as a holder. This is illustrated in Fig. 7a. Next, the mounted fibers are polished horizontally to reach optical quality (λ/50). The samples are polished with a series of 600 and 1200 grid silicon carbide and then using 6μm, 1μm and 0.25μm diamond polishing powder in oil. The typical parameters are reported in Table 3. The polishing machine was configured to 100rpm. Notice that the polishing step is very important since surface roughness strongly impacts both the IR peak intensity and its position when measured in reflectance configuration. This is illustrated in Fig. 8 where the peak is shown for various surface roughnesses. Typically the peak shift (towards smaller wavenumbers) can be as high as 4 cm^{-1} when average surface roughness (RMS) increases from 0.055 to 0.27 microns (Hong 2003).

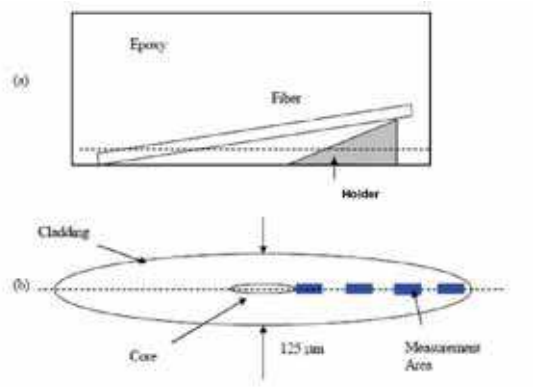

Fig. 7. Schematic diagram for the procedure to create an elongated cross-section of an optical fiber (Hong 2003). a) Mounting of the fiber in epoxy resin at an oblique angle using a thin tapered base. b) Cross-section of the fiber after polishing up to the dotted line indicated in Fig. a.

The polished fibers were subsequently etched for 30 s in 10% HF-10% H_2SO_4 solution to reveal boundaries of the core, inner-cladding and outer-cladding. Finally, the FTIR reflection spectra were recorded by means of standard FTIR spectrometer as shown in Fig. 7b. Spectra have been recorded in the 800 cm^{-1} to 2000 cm^{-1} spectral range with a spectral resolution of 4 cm^{-1} and by averaging 512 scans. The mask size was close to 8 μm x 100 μm resulting in a probe area corresponding to the SMF core only.

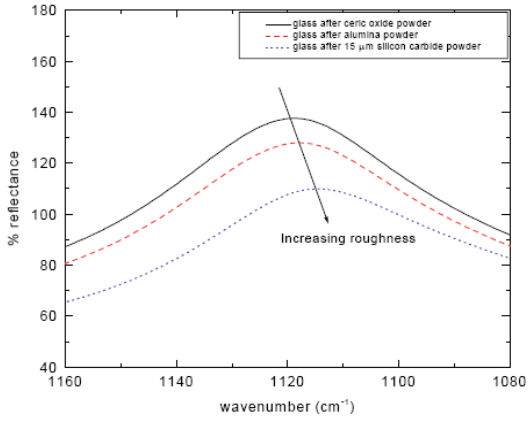

Fig. 8. Shifts in peak positions and intensity of the 1120 cm^{-1} band in IR reflection for GeO_2 doped silica glasses with different surface roughness (Hong 2003).

3.3 Experimental setup

FTIR reflectance spectra were recorded by means of either a Nexus FTIR Spectrometer (Nicolet) or a FTIR Spotlight 300 (Perkin Elmer) equipped with the new technology FPA

(Focal Plan Array) MCT (Mercury Cadmium Telluride) detector. This last instrument provides 6:1 imaging on MCT detector, resulting in nominal resolution of 8 μm. Visible images are recorded under white light LED illumination and are collected via a charge couple device CCD camera to give pictures of arbitrary size and aspect ratio. The desired regions for the IR images are selected from visual images. Typically, we need a few minutes only to perform a mapping of 1 mm² area. The spectra have been recorded in the 800 cm^{-1} to 2000 cm^{-1} spectral range using a spectral resolution of 4 cm^{-1}. The spectra were obtained by averaging only 32 scans (because the signal to noise ratio remains quite high using this technique). When using a standard FTIR spectrometer, spectra have been recorded in the 800 cm^{-1} to 2000 cm^{-1} spectral range with a spectral resolution of 4 cm^{-1} and by averaging 512 scans. In a general manner, the mask size can be reduced down to 20 μm x 20 μm.
Notice that the specular reflection data were collected at a fixed angle of incidence. Indeed, as shown in Fig. 9, a variation in the angle of incidence changes the IR reflection band positions (Almeida 1992; Hong 2003). Thus, the use of the same angle of incidence (i.e. 37° in our experiments) is needed for a reliable determination of fictive temperature.

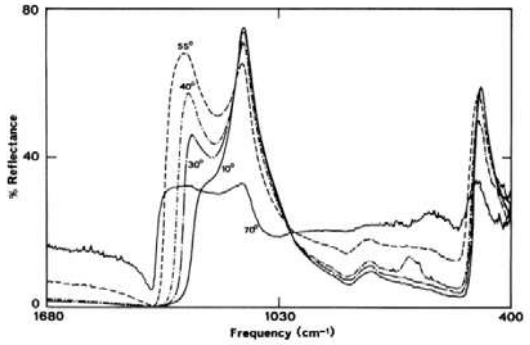

Fig. 9. Specular reflectivity spectra of vitreous silica at different angles of incidence (Almeida 1992).

3.4 Data treatment

An example of the resulting reflectance spectra is shown in Fig. 5. Typically, there is a predominant IR band at 1120 cm^{-1} accompanied by a shoulder at 1200 cm^{-1}. However, one cannot simply choose the wavenumber associated to the largest intensity of an IR band data and call it the peak position because spectral data points are only collected every 2 or 4 cm^{-1}. Indeed, lower spectral resolution results in a much higher noise in the peak determination and thus less precise fictive temperature determination. Hence, the IR peak position was determined by performing a least square polynomial fit and then calculating the minimum of the second derivative using OMNIC@Nicolet or any other fitting software. This is illustrated in Fig. 10. However, one has to be careful because firstly, the sensitivity to noise increases with increasing polynomial degree. Secondly, the choice of the discrete data points used for the fit is very crucial. For instance, if the spectral window width chosen for the fit is too large, shifting the data one step towards higher or lower wavenumber can change the peak position as much as 0.3 cm^{-1}. As the peak position shifts in wavenumber according to the probing area, it is also necessary to change data points for the fit (we cannot keep a fixed

spectral window). Thus, we choose to fix the set of 25 data points around the maximum peak position. Indeed, some interference from a shoulder around 1200 cm^{-1} might occur for larger range. Finally, by changing the set of data or the window width and recalculating the peak position, the stability of the fit is verified. Using this treatment and optimized experimental conditions, we are then able to determine the peak wavenumber with a precision around 0.1 cm^{-1}.

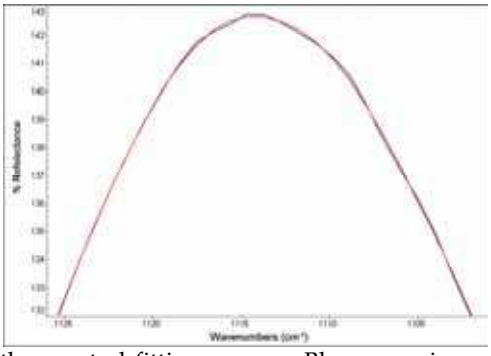

Fig. 10. Illustration of the spectral fitting process. Blue curve is a guide for eye while red curve is for the fit curve.

3.5 Typical results

To summarize, three different methods have been presented to follow the fictive temperature within either MMF or SMF core. In all cases, the 'bond-stretching' vibration mode observed near 1120 cm^{-1} in the FTIR reflection spectra was considered to determine the fictive temperature of the fiber core. Table 4 summarizes the main parameters for each case: type of sample (MMF or SMF, core or cladding), method, spent time (sample preparation + five measurements), spatial resolution, repeatability on T_f measurements (relative error) and number of scans.

For MMF core, there are no peculiar problems due to the large core size (at least 50 microns). We can simply cleave the fiber and probe the core using a standard micro-spectrometer. Typically, the relative error on T_f is lower than ± 20°C. In the case of SMF core, this is slightly more complex due to the small core size i.e. around 8 microns in diameter. From our results, the blaze polished fiber method is the most precise, straight and reliable method, at the expense of a larger time spent.

Specimen	Method	Spent time	Spatial resolution	T_f relative error	Scan times
MMF core	Cleaved	1 hour	30 µm x 30 µm	± 20°C	512
SMF core	Cleaved	1 hour	20 µm x 20 µm	± 30°C	512
SMF core	Cleaved + FPA	1 hour	8 µm x 8 µm	± 40°C	32
SMF core	Blaze polished	6 hours	8 µm x 100 µm	± 20°C	512
SMF inner-cladding	Blaze polished	6 hours	20 µm x 100 µm	± 20°C	512
SMF outer-cladding	Blaze polished	6 hours	40 µm x 100 µm	± 20°C	512

Table 4. Comparison between methods used to estimate the fictive temperature in SMF core.

4. Determination of calibration curves between the IR peak wavenumber and the fictive temperature Tf in silica-based optical fibers

Currently, the main dopants involved in optical telecommunications are, on the one hand, germanium and phosphorus to increase the refractive index, and on the other hand, fluorine to lower the index. The impact of these elements is not limited to a simple variation of refractive index. By doping silica, viscosity, chemical diffusion, absorption, non-linear index etc ... are modified.
Germanium is now the most widely used dopant in silica-based glasses. Indeed, GeO_2 is common for increasing the refractive index of silica (Kao 1983). It is usually found in concentrations ranging from 1 to 30 w%. Up to now, GeO_2 remains also the most prominent dopant to obtain highly photosensitive silica glass to UV light, allowing thus the writing of optical components such as fiber Bragg gratings (Othonos 1997).
Fluorine-doped silica glasses occurs in a variety of technological applications (Gonnet, Nouchi et al. 2007; Matthijsse, Gooijer et al. 2007; Regnier, Kuyt et al. 2008), due mainly to the beneficial changes in optical and physical properties that results from the addition of small quantities of fluorine to pure amorphous silica. Notice that in contrast to Ge and P, which are network formers, fluorine is a network modifier. For optical fiber technology, fluorine is one of only two dopants that decreases the refractive index of silica, the other being boron (Kao 1983). This has resulted in the widespread application of fluorine doping of silica to control the refractive index profile of optical fibers (Kao 1983; Matthijsse, Gooijer et al. 2007). Small contents of F (<1 wt%) have also been introduced to reduce the additional imperfection loss by allowing viscosity-matching. Note that this viscosity-matching technique can also be used with dopants like GeO2 or P2O5 (Kao 1983).
The presence of P_2O_5 reduces strongly the glass viscosity. In optical fiber manufacturing, this allows a relatively low deposition temperature. However, this also leads to a strong increase of the thermal expansion coefficient (and thus a mismatch between P-doped and P-free parts). In addition, the presence of large amounts of P_2O_5 in the core or the cladding can lead to an attenuation increase at long wavelengths (Regnier, Poumellec et al. 2005). Therefore phosphorus is rarely used at high content, and it is then rarely used alone as dopant in silica. That is why many studies on phosphorus have been made in Ge or F co-doped silica glasses (Irven, Harrison et al. 1981). F-P co-doped cladding allows bringing the cladding viscosity closer to that of the core and therefore decreases excess loss. This allows stress reduction at the core-cladding interface and thus reduction in defects and imperfections at the interfaces.

4.1 Literature survey of the calibration curves in silica-based glasses

The radial variation of T_f in optical fiber cross section has been studied recently with some divergent results (Peng, Agarwal et al. 1997; Wissuchek, Ponader et al. 1999; Kim and Tomozawa 2001; Kim, Tomozawa et al. 2001; Helander 2004). One problem is that the reflection peak position varies not only with T_f but also with the material composition (Tajima, Ohashi et al. 1992; Lines 1994; Saito and Ikushima 1998; Saito, Kakiuchida et al. 1998; Tsujikawa, Tajima et al. 2000; Saito and Ikushima 2002; Saito, Yamaguchi et al. 2004). This is an issue as an optical fiber has different compositions in the core and in the cladding surrounding the core. Thus, calibration curves between T_f and the IR band peak position

must be determined for each material composition and especially for Ge, P and F-doped silica.
We have thus reported in Table 5, most of the calibration curves reported in the scientific literature for various silica-based glasses. We have also displayed the experimental temperature range and the corresponding references. The equations displayed in Table 5 are in the form: $\sigma_{1120} = A - B.\ T_f$, where σ (cm^{-1}) is the peak wavenumber (or spectral position) of the Si-O-Si asymmetric stretching band measured in reflectance and T_f (K) is the fictive temperature of the silica glass.

Materials	Calibration equation $\sigma_{1120} = A - B.\ T_f$	Experimental temperature range (K)	Reference
Doped silica			
Ge-doped preform core 3.6 w% 4.7 w % 5.7 w% 6.3 w %	 1130.494 - 0.00709. T_f 1129.325 - 0.00678. T_f 1128.412 - 0.00681. T_f 1127.855 - 0.00687. T_f	1150-1500	Hong 2003 Hong 2004
5 w% Ge-doped bulk	1128.3197 - 0.00673. T_f	1150-1500	
5.3 w% Ge-doped bulk	1128.0034 - 0.00569. T_f	1150-1500	
F-doped Inner cladding	1131.088 - 0.00583. T_f	1150-1600	Kim 2001
Pure silica			
Silica bulk glasses (e.g. infrasil, suprasil 2, suprasil W2, …)	1132.01 - 0.00686. T_f	1150-1500	Hong 2003 Agarwal 1995
Silica bulk glass	1131 - 0.0069. T_f	1350-1750	Le Parc 2002
CVD silica bulk cladding	1131.500 - 0.00742. T_f	1250-1550	Hong 2003 Tomozawa 2005
CVD silica fiber outer-cladding	1132.501 - 0.00669. T_f	1150-1600	Kim 2001 Hong 2003

Table 5. Calibration curves (between T_f and 1120cm^{-1} peak wavenumber measured in reflection) reported in the scientific literature for various silica glasses and optical fibers.

It is worth noticing that no significant difference was found between the different kinds of pure silica glasses i.e. Infrasil, Suprasil 2, Suprasil W2. In contrast, doped silica exhibit strongly different calibration curves, especially for the A coefficient. Unfortunately, the fictive temperature of highly Ge-doped glasses (> 6.7 w % in GeO_2) cannot be estimated reliably due to the lack of calibration curves (Kim, Tomozawa et al. 2001; Hong 2003; Hong, Ryu et al. 2004). Thus, we determine in next section a complete set of calibration curves for germanosilicate glasses for Ge from 1w% to 30w%. Using these curves, we will be able to determine the T_f of Ge-doped glasses whatever the Ge-content may be (between 1 and 30 wt%).

4.2 Determination of calibration curves in Ge-doped silica

4.2.1 Samples preparation and treatments

The specific case of strongly Ge-doped silica has never been reported to our knowledge because it is impossible to cut a highly Ge-doped preform rod into slices without breaking it because of the high level of stress. We have thus circumvented this tricky point by using a graded index preform and by reducing the preform diameter by a factor of 100. A graded index preform with a Ge-doping level up to 30w% was thus stretched into "capillaries"; which are in fact full rods corresponding to the initial preform composition but with a smaller diameter. This allows cutting the capillaries into slices while keeping the spatial resolution to perform many calibration curves for various Ge contents in the same sample. The capillaries were then cut to the desired length to realize the calibration standards. In order to achieve different uniform fictive temperatures in the calibration standards, the samples were held at various temperatures for long time periods, long enough (up to a few 100s hours) to ensure full structural relaxation of the whole preform diameter (i.e. outer-cladding, tube and core). The typical temperatures selected were between 1223 K and 1523 K with an uncertainty around ±2 K (furnace uncertainty). Previous data on bulk silica glass (Sakaguchi and Todoroki 1999; Kim, Tomozawa et al. 2001; Hong 2003) were used to determine appropriate heat treatment times needed to obtain a complete structural relaxation at each heat-treatment temperature. Typical heat-time of bulk silica glasses are shown in Table 6. After heating treatment, these samples were rapidly (< 1s) quenched in water to fix the uniform fictive temperature at the heating temperature (since the relaxation times have been estimated to be a few 100's at these temperatures (Sakaguchi and Todoroki 1999)). Then, the capillaries were polished with a series of 600 and 1200 grid silicon carbide and then to an optically smooth finish with 6µm, 1µm and 0.25µm diamond polishing powder in oil. The polishing machine was configured to 100rpm. Finally, the IR reflection spectra were measured as a function of the radial position (and thus the Ge content) within capillaries.

Temperature	Ge-doped Core	F-doped inner cladding	Pure silica outer cladding
1223K	134h	8h	
1273K	32h	3h	200h
1323K	29h	2h	120h
1373K	8h	1h	66h
1423K	5h	1h	45h
1473K	2h	1h	15h
1523K	1h	1h	3h
1573K			1h

Table 6. Heating treatment conditions of optical fiber capillaries.

4.2.2 Examples of IR reflection spectra in Ge-doped silica

An example of the resulting reflectance spectra is shown in Fig. 11. These spectra were recorded at various locations corresponding to various Ge content of a GI-MMF capillary. We have shown four spectra corresponding to silica outer-cladding (i.e. natural undoped silica), and 5 w%, 15 w% and 25 w% Ge-doped cores. Typically, there is a predominant IR

band at 1120 cm^{-1} accompanied by a shoulder at 1200 cm^{-1}. We can see that the higher is the Ge concentration the lower the wavenumber of TO mode related peak.

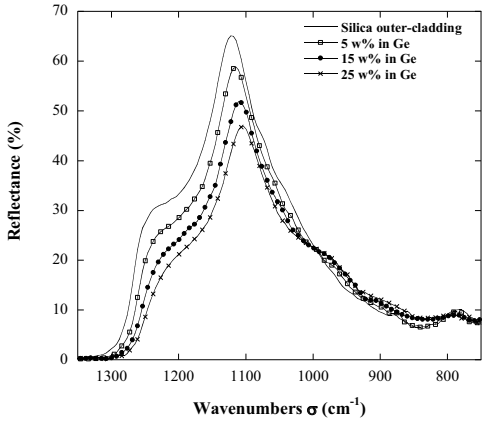

Fig. 11. Typical reflectance spectra corresponding to various location and thus Ge content for the GI-MMF capillary.

4.2.3 2D distribution of the IR peak wavenumber in GI-MMF capillaries annealed at various temperature

Figure 12 displays the 2D distribution of the peak wavenumber σ related to the Si-O-Si asymmetric stretching band recorded in reflection. The circle (black solid line) corresponds to the core part within the capillary. In this figure, the darker the color, the higher the peak wavenumber σ (in cm^{-1}). These results indicate that the concentric distribution of σ is quite constant for a fixed radial position r (constant along a circle) whereas it changes strongly according to the radial position r. In the following, we will extract the radial profiles from these data.

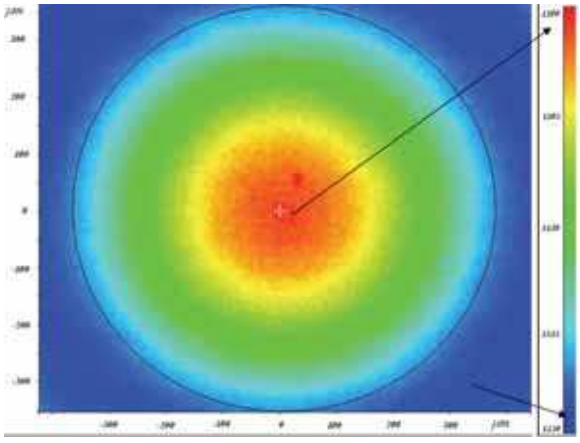

Fig. 12. 2D distribution of the reflectance peak wavenumber σ in the core of the MMF capillaries cross section

4.2.4 Determination of calibration curves: influence of the Ge concentration

In this part, we will extract the data obtained above in order to determine calibration curves between the fictive temperature and the IR reflection peak wavenumber σ for Ge concentrations up to 30 w %. Firstly, we have assumed that the drawing around 2300 K of the preform into rods did not change the germanium concentration profile since it has been shown that it did not change significantly the refractive index profile [20] when compared to our spatial resolution. We have thus converted the radial position r into Ge concentration in the GI-MMF rods using the well-known GI-MMF concentration profile in preform. Now, we are able to follow the evolution of the peak wavenumber according to the fictive temperature T_f (also called the calibration curves or master curves) for various Ge contents.
Figure 13 displays several of these calibration curves for pure silica glass and for various GeO_2 contents from 5 w % to 30w%. In this figure, the symbols are for experimental data while the full lines correspond to best fits of the data using a linear law. The least square regression analysis reveals the following relationship between fictive temperature and IR peak position: $\sigma(Ge, T_f) = A(Ge) - B(Ge) \times T_f$, where the coefficients A and B could depend on the Ge content. Based on those calibration curves, the fictive temperatures of Ge-doped (up to 30 w %) optical fibers can be estimated once the composition of the core is known.
In the following, we will investigate more precisely the effect of the Ge content on the calibration curves parameters: i.e. the ordinate at the origin (coefficient A in cm^{-1}) and the slope B (in cm^{-1} K^{-1}). We have thus extracted these values from the above linear regressions for various Ge concentrations up to 30 w%. Figures 14 and 15 display the evolution of these two parameters according to the Ge concentration together with the error bars. As it can be seen, the coefficient A follows a linear relationship with the Ge content ***(up to 30 w %)***: A = (1129.8 ± 0.1) – (0.469 ± 0.004) x [Ge]. In contrast, the slope B appears to gradually decrease with increasing Ge content. However, this decrease is not significant enough when compared to our measurements uncertainty. In the following, we will thus assume that the slope B is independent on [Ge]: B = 0.0102 ± 0.0002.

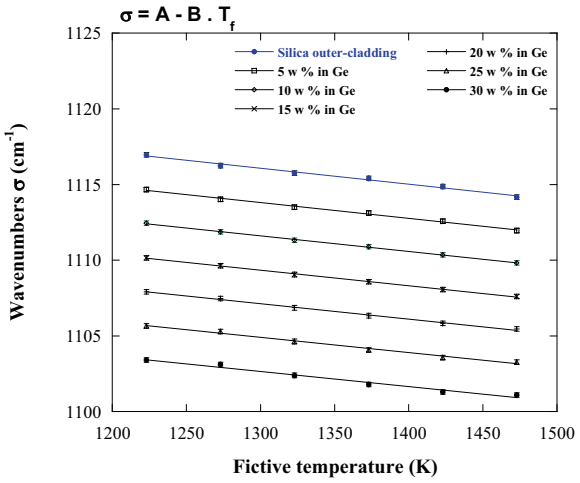

Fig. 13. The relationship between IR peak wavenumber and the fictive temperature for Ge-doped bulk silica for various Ge concentrations.